IEEE Access
Multidisciplinary | Rapid Review | Open Access Journal

IEEE POWER & ENERGY SOCIETY SECTION

Received June 5, 2021, accepted July 12, 2021, date of publication July 16, 2021, date of current version July 26, 2021.

Digital Object Identifier 10.1109/ACCESS.2021.3097802

Measurement-Based Transmission Capability Estimation of Power Grid Using Load Response-Based Equivalent Model

JIAN-HONG LIU, (Member, IEEE), AND JIE-SHENG CHENG
Department of Electrical Engineering, Yuan Ze University, Taoyuan City 32003, Taiwan

Corresponding author: Jian-Hong Liu (jhliu727@saturn.yzu.edu.tw)

This work was supported in part by the Ministry of Science and Technology of Taiwan under Grant MOST 107-2218-E-155-010, Grant MOST 108-2221-E-155 -030, and Grant MOST 110-2221-E-155-037.

ABSTRACT In this paper, the load response-based equivalent model is proposed to develop a more sturdy method for the transmission capability estimation of the power grid. Based on real-time phasor measurement unit (PMU) measurements, the power grid is modelled as the multi-port equivalent model based on the coupled single-port models. The associated critical equivalent branch in the multi-port model is identified and modified by the shaping factor to construct the proposed model. According to the modification, the dissimilarity of the load response index between the critical equivalent branch and the approximate profile of the actual load voltage can indeed be reduced to obtain the perfect matching between the critical load voltage and the actual load voltage. Accordingly, the accurate and sturdy transmission capability estimation can be achieved in the proposed model. Moreover, the proposed model is further extended to design a complete solution algorithm for the limit-induced transmission capability estimation considering generator reactive power limits. Simulations on IEEE 14-bus and IEEE 118-bus test systems are presented to validate the accuracy and the sturdiness of the proposed method.

INDEX TERMS Multi-port equivalent model, cubic spline extrapolation, maximum loading parameter, approximate voltage profile, transmission capability estimation.

I. INTRODUCTION

As intermittent renewable energies have drawn a great deal of attention in the modern power grid, transmission capability estimation of power grid becomes the vital concern for ensuring and maintaining the security operation of the power grid. In renewable energies or any distributed energy resources (DERs), the stochastic nature of the power fluctuation is unpredictable and highly intermittent within various timescales, hourly, daily, and seasonal periods [1]. In the normal operation, the power balance between the instantaneous power generation and the loading consumption of consumers is necessary in order to maintain the voltage stability of power grid, which means that the operating voltage in power grids should remain stable for independent system operators. When renewable energies are integrated into power grids, the associated stochastic factors may lead to the impacts on the voltage stability and present substantial challenge for power system operations [2], [3]. Moreover, the non-dispatchable nature of renewable energies also causes various issues regarding to operation costs and operation reserves in power grids [1]. Voltage stability is an significant topic in power networks since it is the cause of many outages and blackout [4]. Thus, voltage stability estimation, also called transmission capability estimation, becomes critical, being able to provide the efficient stability monitoring of the power transmission to avoid the possible blackout due to uncertainties of renewable energies. Additionally, demand response (DR) is also a branch of the technical applications in transmission capability estimation. DR is defined as profitable and scheduled demand variations in order to increase power system operation stability [5]. With the accurate transmission capability estimation, DR can be appropriately activated to improve the power system operation stability through the reactive resource regulation or the load shedding [6], [7]. In order to meet the applications of fast DR or highly intermittent

The associate editor coordinating the review of this manuscript and approving it for publication was Ning Kang.

renewable resources, the satisfactory, speedy, and reliable technologies of the transmission capability assessment are the urgent demands to ensure the operation stability of a power grid.

Conventionally, several static analysis approaches have been addressed for the transmission capability estimation. Methods based on the fundamental of the static analysis include continuation power flow approaches (CPFLOW) [8]–[10], optimization approaches [12], and direct method [11]. The accuracy in the static analysis-based approaches highly depends on accurate system parameters. As the appealing advantages, all physical constraints can be considered in the static analysis approaches. However, the computational complexities are still the major drawback when the static analysis-based methods are applied in a real-time environment. Due to such deficiency, developing the appropriate real-time techniques for the transmission capability estimation of the power grid has been motivated.

A. LITERATURE REVIEW

With rapid advance of measurement techniques in synchronized phasor measurement units (PMUs), measurement-based approaches have pushed transmission capability monitoring techniques forward and made real-time applications possible. In early time, measurement-based approaches are developed on the basis of a single-port model, where measurements are collected at a single location. Based on the maximum power transfer theorem, the transmission capability can be estimated in a single-port model. Several related works have been represented along the direction. For instance, several applications such as the transmission capability assessment using local measurements [13], the fast local index for the loadability limit estimation [14], and the robust voltage instability predicator [15] have been addressed in a single-port structure. Nevertheless, due to limited measurements in a single location, the accuracy of these methods is restricted.

In order to improve the predicament of the single-port model, multiple-port equivalent models are proposed. By gathering measurements from different locations, multiple-port equivalent models are constructed to model the power grid and perform the wide-area transmission capability monitoring [16]–[18]. In recent advance, coupled single-port models become the famous multi-port equivalent model [18] and are widely extended to several applications in the wide-area transmission capability evaluation of the power grid [19]–[21]. The distinct feature of the coupled single-port models is that there exists the extra coupling impedance, modelling the coupling effect from loads, in the Thevenin impedance of this model. However, the difficulties of modelling the coupling effect under load variations may lead to the inaccurate transmission capability estimation [22]. To deal with such difficulties, the modified coupled single-port models are proposed [22]. The basic idea in the modified coupled single-port models is to modulate the circuit parameters in the existing coupled single-port models by the measured load reactive power sensitivities. In this way, the deficiency of the estimation inaccuracy can indeed be improved. Several extended works along this direction have been shown in [23]–[25]. Although the modified coupled single-port models represent promising results under most normal cases, its accuracy is still restricted due to the limited information of the load reactive power sensitivities.

In order to further advance in the technologies of the real-time transmission capability estimation, the extrapolation-based impedance matching method is represented recently [26]. In this approach, based on few measurements, the variation of the equivalent load impedance for each load is described as the cubic curve and approximated as the cubic polynomial in the cubic spine extrapolation method. By examining the impedance matching point between such cubic load impedance curve and the equivalent network impedance, the accurate transmission capability can be assessed. A few works have extended the fundamental of this method to the applications of the real-time transmission capability assessment [27]–[29]. However, the highly nonlinear variation of the equivalent load impedance is difficult to be analytically formulated as the cubic polynomial through the limited measurements. It definitely obstructs the applicable range of the extrapolation-based impedance matching method in the transmission capability estimation.

B. CONTRIBUTION AND PAPER ORGANIZATION

In order to develop a more sturdy method for the transmission capability estimation of the power grid, the load response-based equivalent model is proposed in this paper. Based on real-time PMU measurements, the power grid is modelled as the multi-port equivalent model based on the coupled single-port models. The associated critical equivalent branch in the multi-port model is identified and modified by the shaping factor to construct the proposed model. According to the modification, the dissimilarity of the load response index between the critical equivalent branch and the approximate profile of the actual load voltage can indeed be reduced to obtain the perfect matching between the critical load voltage and the actual load voltage. Accordingly, the accurate and sturdy transmission capability estimation can be achieved in the proposed model. Moreover, the proposed model is further extended to design a complete solution algorithm for the limit-induced transmission capability estimation considering generator reactive power limits. The accurate estimation results are also received in the proposed solution algorithm. The major contribution in this paper is to propose the load response-based equivalent model which is more sturdy and stands in a wider applicable range for performing the measurement-based transmission capability estimation.

The leftover part of this paper is organized as follows. The multi-port equivalent model of the power grid is introduced in Section II. In Section III, the proposed load response-based equivalent model and its extension to the limit-induced system maximum loading parameter estimation are addressed.

In Section IV, simulation studies on IEEE 14-bus and IEEE 118-bus test systems are presented to validate the accuracy and the sturdiness of the proposed model. Conclusions are finally described in Section V.

II. MULTI-PORT EQUIVALENT MODEL OF POWER GRID

A. COUPLED SINGLE-PORT MODELS

Coupled single-port models are effectual multi-port equivalent models for modelling the power grid [18]. In an interconnected power grid, the injection current and the terminal voltage can be formulated according to the following admittance matrix Y as follows [18]

$$\begin{bmatrix} I_G \\ \bar{I}_L \\ I_T \end{bmatrix} = \begin{bmatrix} Y_{GG} & Y_{GL} & Y_{GT} \\ Y_{LG} & Y_{LL} & Y_{LT} \\ Y_{TG} & Y_{TL} & Y_{TT} \end{bmatrix} \begin{bmatrix} V_G \\ V_L \\ V_T \end{bmatrix} \tag{1}$$

where the notations V and I are the voltage phasor and the current phasor for each bus and can be measured by PMUs. Subscripts, G, L and T, denote generator, load and zero injection buses, respectively. Accordingly, I_G, $\bar{I}_L$, and I_T are the injection current phasors of generator buses, load buses, and zero injection buses while V_G, V_L, and V_T denote the terminal voltage phasors at generator buses, load buses, and zero injection buses. In order to efficiently estimate the voltage phasor and the current phasor of each load bus from real-time PMU measurements, proper PMU placements are assumed to ensure the complete observability of the bulk power grid [30]. Now, our aim is to derive the general expression of the load voltage from (1), which can also be assessed in [18], [22]. First, (1) can be rearranged as the following three formulas for all injection current, as expressed by

$$I_G = Y_{GG}V_G + Y_{GL}V_L + Y_{GT}V_T \tag{2}$$
$$\bar{I}_L = Y_{LG}V_G + Y_{LL}V_L + Y_{LT}V_T \tag{3}$$
$$I_T = Y_{TG}V_G + Y_{TL}V_L + Y_{TT}V_T \tag{4}$$

Since no injection current exists in the zero injection buses, by letting $I_T = 0$ in (4), the terminal voltage of the zero injection buses can be derived as

$$V_T = -Y_{TT}^{-1}(Y_{TG}V_G + Y_{TL}V_L) \tag{5}$$

Furthermore, in (3), by replacing V_T with the terminal voltage expression of (5), (3) can be reformulated as

$$\left(Y_{LT}Y_{TT}^{-1}Y_{TG} - Y_{LG}\right)V_G - \left(Y_{LL} - Y_{LT}Y_{TT}^{-1}Y_{TL}\right)V_L + \bar{I}_L = 0 \tag{6}$$

In (6), by defining the equivalent impedance Z_{LL} with

$$Z_{LL} = (Y_{LL} - Y_{LT}Y_{TT}^{-1}Y_{TL})^{-1} \tag{7}$$

the load voltage equations can be rearranged as the following compact form:

$$V_L = E_{eq} - Z_{LL}I_L \tag{8}$$

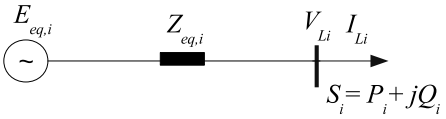

FIGURE 1. Coupled single-port model for the *i*th load bus.

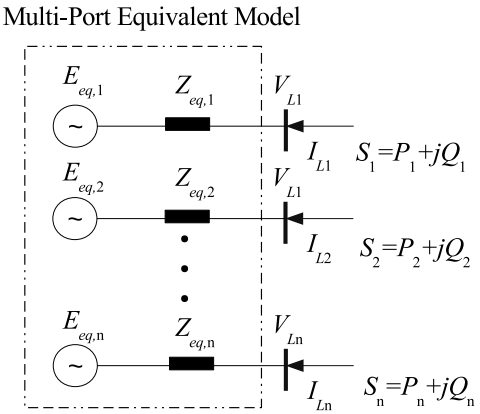

FIGURE 2. Multi-port equivalent model of the power grid.

where $I_L = -\bar{I}_L$ denotes the load current which represents the reversal load injection current flowing into load buses. The equivalent voltage source E_{eq} is defined by

$$E_{eq} = Z_{LL}(Y_{LT}Y_{TT}^{-1}Y_{TG} - Y_{LG})V_G \tag{9}$$

If the coupling term is introduced in the load voltage equations and modelled as an extra impedance [18], (8) can be further extracted to derive the *i*th equivalent branch circuit, as rewritten by

$$\begin{aligned} V_{Li} &= E_{eq,i} - Z_{LLii}I_{Li} - \left(\sum_{j=1,i\neq j}^{n} Z_{LLij}\frac{I_{Lj}}{I_{Li}}\right)I_{Li} \\ &= E_{eq,i} - Z_{LLii}I_{Li} - Z_{coupling,i}I_{Li} \end{aligned} \tag{10}$$

for $i = 1, 2, 3, \ldots, n$, where V_{Li} and I_{Li} represent the voltage and the current at the *i*th load bus. Z_{LLii} is the diagonal component of Z_{LL}, and Z_{LLij} is the $i-j$ element of Z_{LL}. The coupling impedance $Z_{coupling,i}$ represents the coupling effect from other loads. (10) is utilized to represent the coupled single-port model for the *i*th load bus, where the equivalent impedance $Z_{eq,i} = Z_{LLii} + Z_{coupling,i}$ is modelled as the series connection of Z_{LLii} and $Z_{coupling,i}$, and $E_{eq,i}$ denotes the equivalent voltage source [18]. For the *i*th load bus, the corresponding coupled single-port model is depicted in Fig. 1. Furthermore, the multi-port model of the power grid can be constructed by collecting all coupled single-port models, as addressed in Fig. 2.

B. TRANSMISSION CAPABILITY

The transmission capability of the power grid is further estimated in the multi-port equivalent model of the power grid. By applying Kirchhoff's voltage law at the coupled single-port model of the *i*th load bus, the quadratic equation

$F_i(|V_{Li}|, \lambda_i)$ can be derived by

$$F_i(|V_{Li}|, \lambda_i) = |V_{Li}|^4 + b_i|V_{Li}|^2 + c_i = 0 \tag{11}$$

where the coefficients b_i and c_i can be presented by

$$\begin{aligned} b_i &= 2P_iR_{eq,i} + 2Q_iX_{eq,i} - |E_{eq,i}|^2 \\ c_i &= |Z_{eq,i}|^2(P_i^2 + Q_i^2) \end{aligned} \tag{12}$$

The equivalent impedance can be represented as a complex-valued form $Z_{eq,i} = R_{eq,i} + jX_{eq,i}$. In (12), for the ith load bus, the real and reactive loading power are expressed as $P_i = P_{0i} + \lambda_i\overrightarrow{P_i}$ and $Q_i = Q_{0i} + \lambda_i\overrightarrow{Q_i}$ and addressed in the load-increase scenario with the PMU measurements of the base-case real power P_{0i} and reactive power Q_{0i}, the time-varying load directions of $\overrightarrow{P_i}$ and $\overrightarrow{Q_i}$, and the dispersed loading parameter λ_i. For the given dispersed loading parameter λ_i, the equivalent load voltage can be determined in (11) as follows

$$|V_{Li}| = \sqrt{\frac{-b_i + \sqrt{b_i^2 - 4c_i}}{2}} \tag{13}$$

When the quadratic equation $F_i(|V_{Li}|, \lambda_i)$ has a unique solution, the corresponding dispersed loading parameter λ_i reaches its maximum one λ_i^*, as expressed by

$$\lambda_i^* = \frac{-\sigma_{b,i} + \sqrt{\sigma_{b,i}^2 - 4\sigma_{a,i}\sigma_{c,i}}}{2\sigma_{a,i}} \tag{14}$$

where the coefficients are expressed by

$$\begin{aligned} \sigma_{a,i} &= 4(R_{eq,i}\overrightarrow{Q_i} - X_{eq,i}\overrightarrow{P_i})^2 \\ \sigma_{b,i} &= 2(R_{eq,i}Q_{0i} - X_{eq,i}P_{0i})\sigma_a \\ &\quad + 4|E_{eq,i}|^2(R_{eq,i}\overrightarrow{P_i} + X_{eq,i}\overrightarrow{Q_i}) \\ \sigma_{c,i} &= 4(R_{eq,i}Q_{0i} - X_{eq,i}P_{0i}) \\ &\quad + 4|E_{eq,i}|^2(R_{eq,i}P_{0i} + X_{eq,i}Q_{0i}) - |E_{eq,i}|^4 \end{aligned}$$

Exploring all dispersed maximum loading parameters, the smallest one, corresponding to the critical one λ_c^*, is used as the estimation of the system maximum loading parameter λ_{sys}^*, and the transmission capability assessment of the power grid is defined by

$$\lambda_c^* = \min_{i=1\ldots,n} \lambda_i^* \tag{15}$$

where the critical maximum loading parameter λ_c^* corresponds to the critical equivalent branch of coupled single-port models.

C. LOAD RESPONSE INDEX

Referring to (13), the critical load voltage V_{Lc} at the critical equivalent branch is calculated as the function of the critical loading parameter λ_c and depicted in Fig. 3. Corresponding to the critical maximum loading parameter λ_c^*, the boundary critical load voltage is denoted by V_{Lc}^*. Compared with the actual load voltage in Fig. 3, it can be clearly found that the poor decline curve of V_{Lc} in the critical equivalent branch,

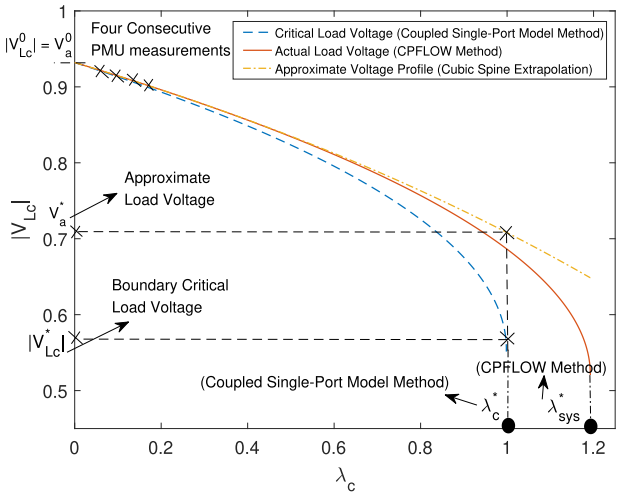

FIGURE 3. Decline curve of the critical load voltage V_{Lc}, the actual load voltage and the approximate voltage profile in the critical equivalent branch. (The actual unlimited system maximum loading parameter λ_{sys}^* approximated by the CPFLOW method, and the unlimited system maximum loading parameter λ_c^* predicted by the coupled single-port model method).

corresponding to the worse curve matching of the critical load voltage with the actual load voltage, may lead to the inaccurate estimation of the system maximum loading parameter. It indicates that the critical equivalent branch is necessary to be modified to eliminate such mismatch. In order to facilitate the reduction of the mismatch, the load response index (LRI) is utilized. LRI is defined by the ratio of the critical load voltage deviation, corresponding the base-case and the maximum loading parameters, to the critical maximum loading parameter, as expressed by

$$LRI = \frac{|V_{Lc}^*| - |V_{Lc}^0|}{\lambda_c^*} \tag{16}$$

where V_{Lc}^0 is the critical load voltage under the critical base-case loading parameter ($\lambda_c = 0$). LRI can be used to quantify the variation of the decline curve of the critical load voltage. Obviously, at the critical equivalent branch, the mismatch between the actual load voltage and the critical load voltage represents the dissimilarity of the associated LRI calculations. Hence, the critical equivalent branch is ready to be modified for eliminating the dissimilarity of the LRI calculations.

III. PROPOSED LOAD RESPONSE-BASED EQUIVALENT MODEL

A. MEASUREMENT-BASED LRI

In the beginning, the LRI calculation of the actual load voltage will be addressed. Since the actual load voltage variation is unknown, only the approximate voltage profile of the actual load voltage can be predicted. In order to accurately obtain the approximate voltage profile of the actual load voltage in the critical equivalent branch, a simple cubic polynomial extrapolation method is utilized. In the sense, the approximate

voltage profile describes the load voltage as the cubic function of the critical loading parameter λ_c in the critical equivalent branch. This cubic function can be expressed by

$$V_a = a_3\lambda_c^3 + a_2\lambda_c^2 + a_1\lambda_c + a_0 \tag{17}$$

where V_a is the approximate load voltage on the approximate voltage profile. Adopting the four sets of the consecutive PMU measurements of the actual load voltage V_{Lc}^a and the critical loading parameter λ_c in the critical equivalent branch, the coefficients a_3, a_2, a_1 and a_0 can be determined by a simple cubic polynomial extrapolation technique. Specifically, the coefficients are calculated by

$$\begin{bmatrix} a_3 \\ a_2 \\ a_1 \\ a_0 \end{bmatrix} = \begin{bmatrix} \lambda_c^3(1) & \lambda_c^2(1) & \lambda_c(1) & 1 \\ \lambda_c^3(2) & \lambda_c^2(2) & \lambda_c(2) & 1 \\ \lambda_c^3(3) & \lambda_c^2(3) & \lambda_c(3) & 1 \\ \lambda_c^3(4) & \lambda_c^2(4) & \lambda_c(4) & 1 \end{bmatrix} \begin{bmatrix} V_{Lc}^a(1) \\ V_{Lc}^a(2) \\ V_{Lc}^a(3) \\ V_{Lc}^a(4) \end{bmatrix} \tag{18}$$

where the number within the bracket "( )" is the time stamp of the four consecutive PMU measurements. Once all coefficients are calculated, the approximate voltage profile of the actual load voltage in the critical equivalent branch can be represented by the cubic polynomial of (17), as depicted in Fig. 3. Furthermore, the measurement-based LRI can be calculated in the approximate voltage profile of the actual load voltage and represented by

$$LRI_m = \frac{V_a^* - V_a^0}{\lambda_c^*} \tag{19}$$

where V_a^* is the approximate load voltage corresponding to the critical maximum loading parameter λ_c^* in the approximate voltage profile, as shown in Fig. 3. Moreover, in the base-case condition, the critical load voltage $|V_{Lc}^0|$ is assumed to be identical to the approximate load voltage V_a^0, as shown in Fig. 3.

B. MODIFICATIONS OF CRITICAL EQUIVALENT BRANCH

Next, our target is to modify the critical equivalent branch according to the measurement-based LRI. In this way, the critical load voltage can properly fit the actual load voltage variation to obtain the accurate estimation of the system maximum loading parameter. In order to achieve effective modifications, the equivalent-preserving modification is considered. In such modification, the critical load voltage V_{Lc} and the load current I_{Lc} maintain invariant after modifying the critical impedance $Z_{eq,c}$ and the critical voltage source $E_{eq,c}$ in the critical equivalent branch. Specifically, the equivalent-preserving modification can be performed through introducing a shaping factor ρ to the critical impedance $Z_{eq,c}$ and the critical voltage source $E_{eq,c}$, as expressed by

$$Z_{eq,c}^D = \rho Z_{eq,c}, \quad E_{eq,c}^D = V_{Lc} + Z_{eq,c}^D I_{Lc} \tag{20}$$

Due to the modifications, the quadratic equation in (11) will be accordingly modified and rearranged as $\bar{F}_c(|V_{Lc}|, \lambda_c, \rho)$ in the modified critical equivalent branch. By taking the partial derivative on $\bar{F}_c(|V_{Lc}|, \lambda_c, \rho)$ with respect to $|V_{Lc}|$ and ρ, the associated sensitivity formula can be derived as

$$\frac{\partial \bar{F}_c}{\partial |V_{Lc}|}\Delta|V_{Lc}| + \frac{\partial \bar{F}_c}{\partial \rho}\Delta\rho = 0 \tag{21}$$

where two sensitivity terms can be expressed by

$$\begin{aligned} \frac{\partial \bar{F}_c}{\partial |V_{Lc}|} &= 2|V_{Lc}|^2 + 2\rho(P_c R_{eq,c} + Q_c X_{eq,c}) - |V_{Lc}^0|^2 \\ &\quad - \rho(Z_{eq,c} I_{Lc}^0 \overline{V_{Lc}^0} + \overline{Z_{eq,c}}\,\overline{I_{Lc}^0} V_{Lc}^0) - \rho^2 |Z_{eq,c}|^2 |I_{Lc}^0|^2 \\ \frac{\partial \bar{F}_c}{\partial \rho} &= 2|V_{Lc}|^2(P_c R_{eq,c} + Q_c X_{eq,c} - \rho|Z_{eq,c}|^2|I_{Lc}^0|^2) \\ &\quad - |V_{Lc}|^2(Z_{eq,c} I_{Lc}^0 \overline{V_{Lc}^0} + \overline{Z_{eq,c}}\,\overline{I_{Lc}^0} V_{Lc}^0) \\ &\quad + 2\rho|Z_{eq,c}|^2(P_c^2 + Q_c^2) \end{aligned} \tag{22}$$

where $R_{eq,c}$ and $X_{eq,c}$ are the real and imaginary parts of the critical impedance $Z_{eq,c}$. The base-case critical load current can be expressed by I_{Lc}^0. The complex conjugates with respect to $Z_{eq,c}$, V_{Lc}^0, and I_{Lc}^0 are denoted by $\overline{Z_{eq,c}}$, $\overline{V_{Lc}^0}$, and $\overline{I_{Lc}^0}$ respectively. Lying in the critical maximum loading parameter λ_c^*, (21) can be further rearranged as the sensitivity of the shaping factor to LRI, as expressed by

$$\Delta\rho = -\lambda_c^* \frac{\frac{\partial \bar{F}_c}{\partial |V_{Lc}|}}{\frac{\partial \bar{F}_c}{\partial \rho}}\Bigg|_{\substack{\lambda_c=\lambda_c^* \\ |V_{Lc}|=|V_{Lc}^*|}} \quad \Delta LRI = S_\rho\Big|_{\substack{\lambda_c=\lambda_c^* \\ |V_{Lc}|=|V_{Lc}^*|}} \Delta LRI \tag{23}$$

where S_ρ is defined as the shaping factor sensitivity. Explicitly, (23) can be interpreted that the assigned LRI deviation requires the necessary correction of the shaping factor.

Now, the major effort is to force the LRI in the modified critical equivalent branch to match the measured one, LRI_m, through placing the proper shaping factor. In this way, the dissimilarity of LRI between the critical equivalent branch and the actual load voltage profile can be effectively eliminated. In order to calculate the proper shaping factor to eliminate such dissimilarity of LRI, (23) can be performed iteratively.

For the kth elimination of the dissimilarity of LRI, the correction increment of the shaping factor is determined by

$$\Delta\rho^{(k)} = S_\rho\Big|_{\substack{\lambda_c=\lambda_c^* \\ |V_{Lc}|=|V_{Lc}^*|^{(k)} \\ \rho=\rho^{(k)}}} \Delta LRI^{(k)} \tag{24}$$

where $\Delta LRI^{(k)} = LRI_m - LRI^{(k)}$ represents the dissimilarity of LRI at the kth iteration. $LRI^{(k)}$ denotes the LRI under the corrected shaping factor $\rho^{(k)}$ in the modified critical equivalent branch at the kth iteration. $|V_{Lc}^*|^{(k)}$ is the critical load voltage magnitude, corresponding to the critical maximum load parameter λ_c^*, in the modified critical equivalent branch at the kth iteration. It is notable that the corrected shaping factor is initiated by $\rho^{(k=0)} = 1$. At the kth iteration, the corrected shaping factor can be updated by

$$\rho^{(k+1)} = \rho^{(k)} + \eta\Delta\rho^{(k)} \tag{25}$$

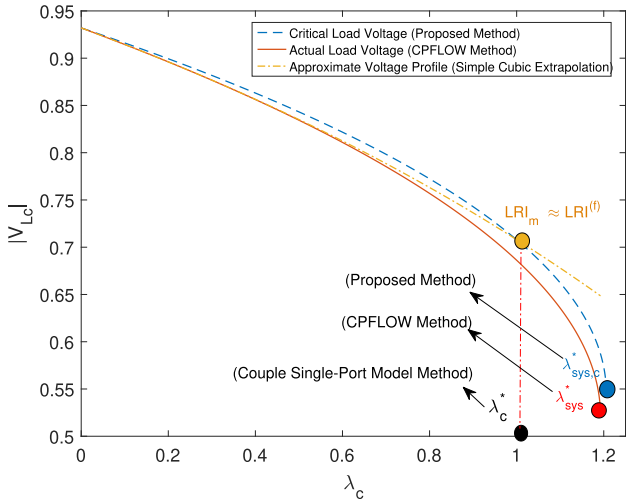

FIGURE 4. The elimination of the dissimilarity of LRI between the critical equivalent model and the actual load voltage. (The actual unlimited system maximum loading parameter λ^*_{sys} approximated by the CPFLOW method, the unlimited system maximum loading parameter λ^*_c predicted by the coupled single-port model method, and the unlimited system maximum loading parameter $\lambda^*_{sys,c}$ estimated by the proposed method).

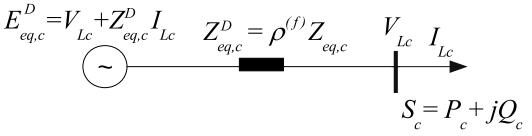

FIGURE 5. Load response-based equivalent model.

where η is the step length of the correction. The corrected shaping factor is designed to modify the critical equivalent branch. During each iteration, if $\Delta LRI^{(k)} < \epsilon$ encounters with the required tolerance ϵ, the correction process will stop to generate the final corrected shaping factor $\rho^{(f)}$. As a result, the dissimilarity of LRI between the critical equivalent branch and the actual load voltage can be effectively eliminated, as depicted in Fig. 4. Ultimately, $\rho^{(f)}$ is utilized to form the modified critical equivalent branch with the modified critical impedance $Z^D_{eq,c} = \rho^{(f)} Z_{eq,c}$ and the modified critical voltage source $E^D_{eq,c} = V_{Lc} + Z^D_{eq,c} I_{Lc}$. This modified critical equivalent branch is defined as the proposed load response-based equivalent model, as depicted in Fig. 5. In the proposed load response-based equivalent model, the accurate estimation of the system maximum loading parameter is expected, as demonstrated by the transmission capability estimation $\lambda^*_{sys,c}$ in Fig. 4.

C. ESTIMATION OF LIMIT-INDUCED SYSTEM MAXIMUM LOADING PARAMETER

In the proposed model, the transmission capability estimation $\lambda^*_{sys,c}$ is characterized as the unlimited system maximum loading parameter estimation in which no physical constraint is considered. To meet practical applications, the proposed model will be extended to estimate the limit-induced system maximum loading parameter caused by generator reactive power limits. The previous literature has found that the system loading parameter λ_{sys} is the approximate quadratic function of the generator reactive power generation [31]. That is, for the kth generator, the reactive power generation $Q_{G,k}$ can be represented by

$$\lambda_{sys} = a_k Q^2_{G,k} + b_k Q_{G,k} + c_k \tag{26}$$

where the coefficients a_k, b_k, and c_k can be evaluated by the extrapolation technique using three measurement sets of $Q_{G,k}$ and λ_{sys}, as addressed in the following matrix form

$$\begin{bmatrix} a_k \\ b_k \\ c_k \end{bmatrix} = \begin{bmatrix} Q^2_{G,k}(1) & Q_{G,k}(1) & 1 \\ Q^2_{G,k}(2) & Q_{G,k}(2) & 1 \\ Q^2_{G,k}(3) & Q_{G,k}(3) & 1 \end{bmatrix}^{-1} \begin{bmatrix} \lambda_{sys}(1) \\ \lambda_{sys}(2) \\ \lambda_{sys}(3) \end{bmatrix} \tag{27}$$

where the number within the bracket "()" denotes the time stamp of the three consecutive PMU measurements. The quadratic curves of the system loading parameter verse the kth generator reactive power can be depicted in Fig. 6. Such quadratic curves can be categorized into two variation cases, (i) upper variation case and (ii) lower variation case, for the given generator reactive power limit inequality $Q_{min,k} \le Q_{G,k} \le Q_{max,k}$. Both variation cases define the extreme generator reactive power $Q^*_{C,k}$ corresponding to the estimated unlimited system maximum loading parameter $\lambda^*_{sys,c}$. The extreme generator reactive power $Q^*_{C,k}$ can be calculated by

$$Q^*_{C,k} = \frac{-b_k + \sqrt{b_k^2 - 4a_k(c_k - \lambda^*_{sys,c})}}{2a_k} \tag{28}$$

In the upper variation case, the generator reactive power increases with the loading parameter. As depicted in Fig. 6, if the condition $Q^*_{C,k} > Q_{max,k}$ exists, the power grid will suffer the limit-induced voltage instability due to hitting the maximum generator reactive power limit of the kth generator as the generator reactive power increases. Corresponding to the maximum generator reactive power limit

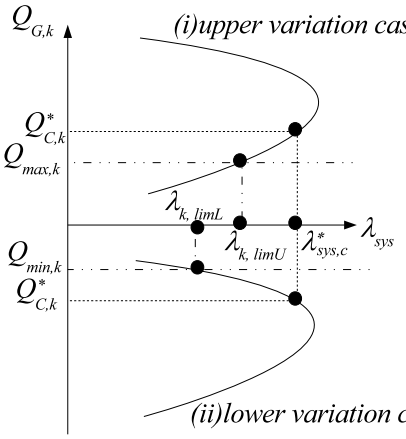

FIGURE 6. The quadratic curves of the system loading parameter verse the kth generator reactive power in the upper and lower variation cases.

$Q_{max,k}$, the upper limit-induced maximum loading parameter $\lambda_{k,limU}$ is reported. Similarly, in the lower variation case, the kth generator reactive power decreases and hits the minimum reactive power limit $Q_{min,k}$ if the condition $Q^*_{C,k} < Q_{min,k}$ stands. In this case, the lower limit-induced maximum loading parameter $\lambda_{k,limL}$, corresponding to the minimum generator reactive power limit $Q_{min,k}$, is recorded. In this way, either $\lambda_{k,limU}$ or $\lambda_{k,limL}$ is treated as a candidate of the limit-induced system maximum loading parameter estimation. Exploring all generators, the estimated limit-induced system maximum loading parameter $\lambda^*_{sys,lim,c}$ can be determined by

$$\lambda^*_{sys,lim,c} = \min_j \lambda^*_{j,lim} \tag{29}$$

where $\lambda^*_{j,lim}$ is the jth candidate of the limit-induced system maximum loading parameter estimation. If no candidate is found, it reveals that the transmission capability estimation is unlimited and reported by $\lambda^*_{sys,c}$. Otherwise, the transmission capability estimation appears limited-induced and is reported by $\lambda^*_{sys,lim,c}$. Also, it is worthy to notice that PV-type generator buses will change to PQ-type load buses when generators hit reactive power limits. As a result, the generator reactive power generation is fixed at its reactive power limit while its real power generation keeps increasing. Due to the addition of new load buses, the admittance matrix in (1) needs to be repartitioned and is used to reconstruct the proposed load response-based equivalent model. Then, the proposed model is further extended to perform the limit-induced transmission capability estimation. Here, for the transmission capability estimation of the power grid, a complete solution algorithm is summarized as follows:

1) If generators hit the reactive power limits, the PV-type generator buses change to PQ-type, and the repartition in the admittance matrix of (1) is performed to recalculate the equivalent impedance. Otherwise, go to next step.
2) Construct the load response-based equivalent model and perform the unlimited system maximum loading parameter estimation $\lambda^*_{sys,c}$.
3) Using $\lambda^*_{sys,c}$ to explore all candidates of the limit-induced system maximum loading parameter estimation for all generators.
4) If candidates are empty, the transmission capability estimation appears unlimited and is reported by $\lambda^*_{sys,c}$. Otherwise, the smallest candidate is utilized as the limit-induced system maximum loading parameter estimation $\lambda^*_{sys,lim,c}$. for the limit-induced transmission capability assessment of the power grid.

IV. SIMULATION RESULTS

In this section, the numerical simulations are performed on IEEE 14-bus and IEEE 118-bus test systems to verify the accuracy and sturdiness of the proposed load response-based equivalent model in the transmission capability estimation of the power grid.

TABLE 1. Dispersed maximum loading parameters λ_i^* of the eight equivalent branches (E.B.) corresponding to the eight load buses under the three loading conditions in IEEE 14-bus system. (The eight dispersed maximum loading parameters, λ_1^* to λ_8^*, estimated in the eight equivalent branches, E.B.1 to E.B.8, corresponding to the eight load buses).

Loading Conditions	E.B.1 λ_1^*	E.B.2 λ_2^*	E.B.3 λ_3^*	E.B.4 λ_4^*	E.B.5 λ_5^*	E.B.6 λ_6^*
Light	4.4	4.356	19.381	14.072	0.998	5.278
Moderate	2.62	2.511	12.503	8.99	0.402	3.192
Heavy	1.439	1.285	7.954	5.625	0.05	1.812
Loading Conditions	E.B.7 λ_7^*	E.B.8 λ_8^*				
Light	2.926	3.081				
Moderate	1.63	1.704				
Heavy	0.776	0.793				

A. IEEE 14 BUS SYSTEM

In this case, generator reactive power limits are not considered in the simulation, and the transmission capability estimation is unlimited. In the designed simulation, eight loads are installed in IEEE 14-bus test system and assigned the following three loading conditions:

1) Light loading condition: The total real and reactive power are amounted to 1.1 p.u. and 1 p.u..
2) Moderate loading condition: The total real and reactive power are increased to 1.607 p.u. and 1.458 p.u..
3) Heavy loading condition: The total real and reactive power are further raised to 2.24 p.u. and 2.03 p.u..

First, the critical equivalent branch is identified. Table.1 shows the dispersed maximum loading parameters of the eight equivalent branches corresponding to the eight load buses under the three loading conditions. It can be clearly observed that there exists the smallest dispersed maximum loading parameter at the 5th equivalent branch. According to the definition of the critical equivalent branch in (15), the 5th equivalent branch is representative and defined as the critical equivalent branch. Thus, in the simulation, the critical equivalent branch is addressed at the 5th load bus and further modified as the proposed load response-based equivalent model. Fig. 7 to Fig. 9 depict the decline curve of the critical load voltage and the actual load voltage in the proposed load response-based equivalent model under light, moderate and heavy loading cases, respectively. In these figures, λ^*_{sys} represents the actual unlimited system maximum loading parameter, approximated by the CPFLOW method, and $\lambda^*_{sys,c}$ denotes the estimated one in the proposed load response-based equivalent model. Obviously, by eliminating the dissimilarity of LRI between the actual load voltage and the critical load voltage, the decline curve of the critical load voltage in the proposed model appropriately matches the actual load voltage profile, therefore, the proposed method can report the accurate unlimited system maximum loading parameter.

Table. 2 summarizes the comparison of the unlimited system maximum loading parameter estimation between the proposed model and the existing methods under the three loading conditions. Here, the existing methods, including

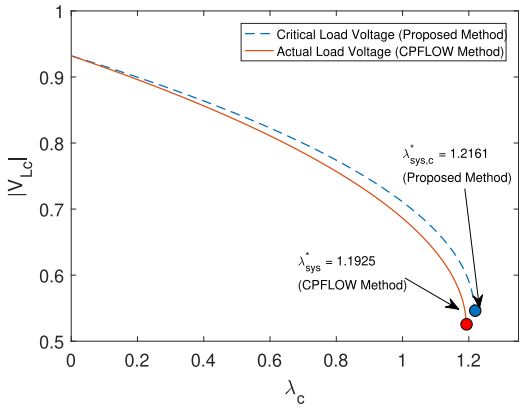

FIGURE 7. Decline curve of the critical load voltage and the actual load voltage in the load response-based equivalent model under the light loading case of IEEE 14-bus test system. (Unlimited system maximum loading parameter $\lambda^*_{sys,c}$ estimated by the proposed load response-based equivalent model, and the actual unlimited system maximum loading parameter λ^*_{sys} approximated by the CPFLOW method).

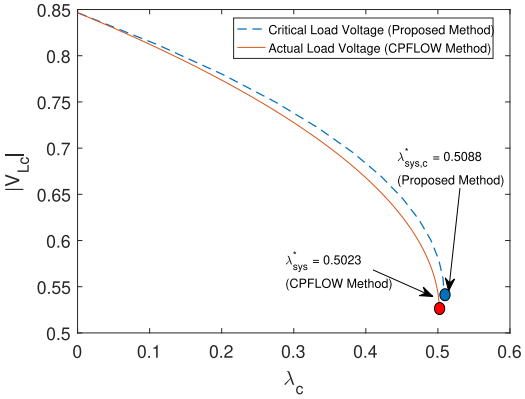

FIGURE 8. Decline curve of the critical load voltage and the actual load voltage in the load response-based equivalent model under the moderate loading case of IEEE 14-bus test system. (Unlimited system maximum loading parameter $\lambda^*_{sys,c}$ estimated by the proposed load response-based equivalent model, and the actual unlimited system maximum loading parameter λ^*_{sys} approximated by the CPFLOW method).

the coupled single-port model method [18], the modified coupled single-port model method [22], and the existing extrapolation-based impedance matching method [26], are addressed for the comparison of the accuracy. The mismatches in Table. 2 are evaluated in term of the degree of the difference between the actual unlimited system maximum loading parameter λ^*_{sys} and ones of the existing methods. In Table. 2, it can be clearly observed that only under the moderate loading condition, the estimated unlimited system maximum loading parameter $\lambda^*_{sys,e}$ in the existing extrapolation-based impedance matching method is more accurate with the mismatch of -0.709% and slightly better than the one in the proposed model. Nevertheless, except this optimistic result, the estimated unlimited system maximum loading parameters in these existing methods have the significant mismatches while the mismatch in the proposed model is not larger than $\pm 2\%$. In addition, Table. 2 also shows

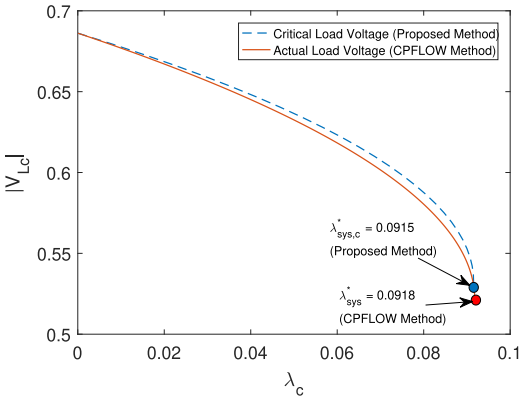

FIGURE 9. Decline curve of the critical load voltage and the actual load voltage in the load response-based equivalent model under the heavy loading case of IEEE 14-bus test system. (Unlimited system maximum loading parameter $\lambda^*_{sys,c}$ estimated by the proposed load response-based equivalent model, and the actual unlimited system maximum loading parameter λ^*_{sys} approximated by the CPFLOW method).

TABLE 2. Comparison of unlimited system maximum loading parameter estimation between the proposed model and the existing methods under three loading conditions. (Unlimited system maximum loading parameters, $\lambda^*_{sys,co}$, $\lambda^*_{sys,mco}$, $\lambda^*_{sys,e}$, and $\lambda^*_{sys,c}$, estimated respectively by the coupled single-port model method, the modified coupled single-port model method, the existing extrapolation-based impedance matching method, and the proposed load response-based method. The actual unlimited system maximum loading parameter λ^*_{sys} approximated by the CPFLOW method).

Loading conditions	CPFLOW (actual) λ^*_{sys}	Coupled method $\lambda^*_{sys,co}$	Modified Coupled method $\lambda^*_{sys,mco}$	Extrapolation method $\lambda^*_{sys,e}$	Proposed method $\lambda^*_{sys,c}$
IEEE 14 Bus					
Light	1.1925	0.998	1.05	0.7242	1.2161
Moderate	0.5023	0.402	0.42	0.4987	0.5088
Heavy	0.0918	0.05	0.055	0.1149	0.0915
Loading conditions		Coupled method Mismatch$_{co}$	Modified Coupled method Mismatch$_{mco}$	Extrapolation method Mismatch$_e$	Proposed method Mismatch$_c$
IEEE 14 Bus					
Light		-16.3 %	-12 %	-39.26%	1.97%
Moderate		-20 %	-16.3 %	-0.709%	1.30%
Heavy		-45.5 %	-40 %	25.2%	-0.27%
	Average mismatch	27.26 %	22.76 %	21.6%	1.2%
Loading conditions	CPFLOW (actual) λ^*_{sys}	Coupled method $\lambda^*_{sys,co}$	Modified Coupled method $\lambda^*_{sys,mco}$	Extrapolation method $\lambda^*_{sys,e}$	Proposed method $\lambda^*_{sys,c}$
IEEE 118 Bus					
Light	4.4408	2.41	2.86	0.5673	4.3242
Moderate	0.3089	0.107	0.153	0.306	0.3114
Heavy	0.1228	0.06	0.069	0.1634	0.1252
Loading conditions		Coupled method Mismatch$_{co}$	Modified Coupled method Mismatch$_{mco}$	Extrapolation method Mismatch$_e$	Proposed method Mismatch$_c$
IEEE 118 Bus					
Light		-45.7 %	-35.5 %	-87.22%	-2.62%
Moderate		-65.3 %	-50.4 %	0.54%	0.8%
Heavy		-51.1 %	-43.8 %	33.07 %	2 %
	Average mismatch	54.03 %	43.2 %	40.27%	1.8%

that the negligible average mismatch of 1.2% stands for the proposed model, compared with much higher ones in these existing methods. It can be found that the proposed model

TABLE 3. CPU execution time of the proposed method and the existing methods in IEEE 14 bus and IEEE 118 bus test systems.

Test Systems	CPFLOW method	Coupled method	Modified Coupled method	Extrapolation method	Proposed method
IEEE 14 bus system	0.588 s	0.061 s	0.062 s	0.06 s	0.063 s
IEEE 118 bus system	1.262 s	0.203 s	0.205 s	0.201 s	0.207 s

is more sturdy and accurate than the existing methods for the transmission capability estimations of the power grid. Besides, the CPU execution time in the proposed method and the concerned existing methods is also studied in IEEE 14-bus system, as shown in Table. 3. It can be clearly observed that the measurement-based approaches, the existing methods and the proposed method, have an more efficient and speedy CPU execution time than the conventional model-based CPFLOW method for the transmission capability estimation. Thus, the measurement-based approaches can meet the real-time applications for the transmission capability estimations of the power grid.

B. IEEE 118 BUS SYSTEM

In the case study of IEEE 118 bus test system, both unlimited and limit-induced transmission capability estimations will be performed and addressed as follows.

1) CASE STUDY UNDER NO GENERATOR REACTIVE POWER LIMITS

In this case study, the unlimited transmission capability estimation is performed. In the simulation, fifty-three loads are assigned the specific loading conditions in IEEE 118-bus test system. In the design, the simulation considers the following three system loading conditions:

1) Light loading condition: The total real and reactive power are amounted to 5.6 p.u. and 5.5 p.u..
2) Moderate loading condition: The total real and reactive power are increased to 20.862 p.u. and 20.625 p.u..
3) Heavy loading condition: The total real and reactive power are further raised to 25.58 p.u. and 25.3 p.u..

Under the above specifications, the critical equivalent branch is located at the 10th load bus and further modified as the proposed load response-based equivalent model. In the simulation, the unlimited system maximum loading parameter estimation can be accurately reported in the proposed model, as listed in Table. 2. On the contrary, the inaccurate estimation results are represented in the existing methods under most loading conditions. Especially, under the light loading condition, there exists the much higher mismatch of -87.22% in the existing extrapolation-based impedance matching method, as recorded in Table. 2. Moreover, the average mismatches are also evaluated. Table. 2 shows that the proposed model has the lower average mismatch of 1.8% while the higher ones exist in these existing methods. It shows that the proposed model is more sturdy than the existing methods in the transmission capability assessment. Moreover, regarding to IEEE 118-bus system, the CPU execution time in the proposed method and the concerned existing methods is depicted in Table. 3. It can reveal that the measurement-based approaches are more efficient and speedy than the conventional model-based CPFLOW method for the transmission capability estimation of power grids.

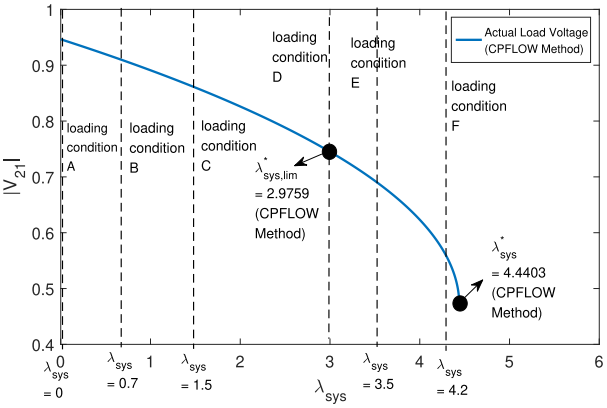

FIGURE 10. Decline curve of the actual voltage magnitude of the bus 21 in IEEE 118-bus test system. (The actual limited system maximum loading parameter $\lambda^*_{sys,lim}$ and the actual unlimited system maximum loading parameter λ^*_{sys}, approximated by the CPFLOW method).

2) CASE STUDY UNDER GENERATOR REACTIVE POWER LIMITS

Generator reactive power limits are considered in this case study, and the limit-induced transmission capability estimation is performed accordingly. In this case study, the critical equivalent branch corresponds to the bus 21. Fig. 10 shows the decline curve of the voltage magnitude at the bus 21 when the system loading parameter increases. In Fig. 10, when the loading parameter has the increase of 2.9759, there exists the limit-induced voltage instability caused by hitting the generator reactive power upper limit 1.23 p.u. of the generator at the bus 85. It is noticed that the generator at the bus 85 is the only one violating the reactive power limit. Accordingly, the limit-induced system maximum loading parameter is represented by $\lambda^*_{sys,lim} = 2.9759$, as shown in Fig. 10. When the power grid encounters the limit-induced voltage instability, the operation mode of the associated PV-type generators changes to the PQ-type load operation by fixing the reactive power generation. As the system load is further increased, the unlimited voltage instability occurs at the system maximum loading parameter $\lambda^*_{sys} = 4.4403$, as illustrated in Fig. 10.

Subsequently, the proposed solution algorithm will be examined under the given six loading conditions. As shown in Fig. 10, the six loading conditions, A to F, correspond to the six system loading parameters, $\lambda_{sys} = 0$, 0.7, 1.5, 2.9759, 3.5 and 4.2, respectively. At the loading conditions A to C, the solution algorithm is applied to produce the estimated limit-induced system maximum loading parameters $\lambda^*_{sys,lim,c}$ with the lower average mismatch of 0.117%, as represented in Table. 4. Table. 4 lists the estimated unlimited and limit-induced system maximum loading parameters under

TABLE 4. Comparison of unlimited and limit-induced system maximum loading parameter estimation between the proposed model and the existing method. (Unlimited and limit-induced system maximum loading parameters, $\lambda^*_{sys,c}$ and $\lambda^*_{sys,lim,c}$, estimated by the proposed load response-based method. Actual unlimited and limit-induced system maximum loading parameters, λ^*_{sys} and $\lambda^*_{sys,lim}$, approximated by the CPFLOW method).

Loading conditions	Proposed method $\lambda^*_{sys,lim,c}$	CPFLOW (actual) $\lambda^*_{sys,lim}$	Proposed method Mismatch
Limit-induced estimation			
A	2.9713	2.9759	-0.154%
B	1.4745	1.4759	-0.094%
C	2.2734	2.2758	-0.105%
		Average mismatch	0.117%
Loading conditions	Proposed method $\lambda^*_{sys,c}$	CPFLOW (actual) λ^*_{sys}	Proposed method Mismatch
Unlimited estimation			
D	1.4368	1.4644	-1.884%
E	0.91	0.94021	-3.213%
F	0.2446	0.24027	1.802%
		Average mismatch	2.29%

the proposed solution algorithm. Furthermore, at the loading conditions D to F, an acceptable average mismatch of 2.29% is also received for the unlimited system maximum loading parameter estimations. In summary, the proposed solution algorithm is more sturdy and accurate for either limited or limit-induced transmission capability estimation.

V. CONCLUSION

In this paper, the load response-based equivalent model is proposed for the measurement-based transmission capability estimation of the power grid. Based on real-time PMU measurements, the critical equivalent branch of coupled single-port models is identified and modified by a shaping factor to construct the proposed model. The shaping factor can be determined by the successful elimination of the dissimilarity of the LRI between the critical load voltage and the approximate voltage profile of the actual load voltage in the critical equivalent branch. In the proposed model, the decline curve of the critical load voltage can perfectly match the actual load voltage profile so that the accurate transmission capability estimation of the power grid can be achieved. Moreover, the proposed model is further extended to design a complete solution algorithm for the limit-induced transmission capability estimation considering generator reactive power limits. The accurate estimation results are also received in the designed solution algorithm. Simulation results on IEEE 14-bus and IEEE 118-bus test systems are presented to validate the accuracy and the sturdiness of the proposed model.

REFERENCES

[1] P. Vijayan, S. Sarkar, and V. Ajjarapu, "A novel voltage stability assessment tool to incorporate wind variability," in *Proc. IEEE Power Energy Soc. Gen. Meeting*, Jul. 2009, pp. 1–8.

[2] J. Zhao, Y. Bao, and G. Chen, "Probabilistic voltage stability assessment considering stochastic load growth direction and renewable energy generation," in *Proc. IEEE Power Energy Soc. Gen. Meeting*, Aug. 2018, pp. 1–5.

[3] Y. Wang, H.-D. Chiang, and T. Wang, "A two-stage method for assessment of voltage stability in power system with renewable energy," in *Proc. IEEE Electr. Power Energy Conf.*, Aug. 2013, pp. 1–6.

[4] K. Liu, W. Sheng, L. Hu, Y. Liu, X. Meng, and D. Jia, "Simplified probabilistic voltage stability evaluation considering variable renewable distributed generation in distribution systems," *IET Gener., Transmiss. Distrib.*, vol. 9, no. 12, pp. 1464–1473, Sep. 2015.

[5] M. B. Wafaa and L. Dessaint, "Multi-objective stochastic optimal power flow considering voltage stability and demand response with significant wind penetration," *IET Gener., Transmiss. Distrib.*, vol. 11, no. 14, pp. 3499–3509, Sep. 2017.

[6] Y. Dong, X. Xie, K. Wang, B. Zhou, and Q. Jiang, "An emergency-demand-response based under speed load shedding scheme to improve short-term voltage stability," *IEEE Trans. Power Syst.*, vol. 32, no. 5, pp. 3726–3735, Sep. 2017.

[7] Y. Dong, X. Xie, W. Shi, B. Zhou, and Q. Jiang, "Demand-response-based distributed preventive control to improve short-term voltage stability," *IEEE Trans. Smart Grid*, vol. 9, no. 5, pp. 4785–4795, Sep. 2018.

[8] H. D. Chiang, A. J. Flueck, K. S. Shah, and N. Balu, "CPFLOW: A practical tool for tracing power system steady-state stationary behavior due to load and generation variations," *IEEE Trans. Power Syst.*, vol. 10, no. 2, pp. 623–633, May 1995.

[9] C. A. Canizares, F. L. Alvarado, C. L. DeMarco, I. Dobson, and W. F. Long, "Point of collapse methods applied to AC/DC power systems," *IEEE Trans. Power Syst.*, vol. 7, no. 2, pp. 673–683, May 1992.

[10] V. Ajjarapu and C. Christy, "The continuation power flow: A tool for steady state voltage stability analysis," *IEEE Trans. Power Syst.*, vol. 7, no. 1, pp. 416–422, Feb. 1992.

[11] I. Dobson and L. Lu, "New methods for computing a closest saddle node bifurcation and worst case load power margin for voltage collapse," *IEEE Trans. Power Syst.*, vol. 8, no. 3, pp. 905–913, Aug. 1993.

[12] G. D. Irisarri, X. Wang, J. Tong, and S. Mokhtari, "Maximum loadability of power systems using interior point nonlinear optimization method," *IEEE Trans. Power Syst.*, vol. 12, no. 1, pp. 6162–6172, Feb. 1997.

[13] K. Vu, M. M. Begovic, D. Novosel, and M. M. Saha, "Use of local measurements to estimate voltage-stability margin," *IEEE Trans. Power Syst.*, vol. 14, no. 3, pp. 1029–1035, Aug. 1999.

[14] M. Parniani and M. Vanouni, "A fast local index for online estimation of closeness to loadability limit," *IEEE Trans. Power Syst.*, vol. 25, no. 1, pp. 584–585, Feb. 2010.

[15] J. Zhao, Z. Wang, C. Chen, and G. Zhang, "Robust voltage instability predictor," *IEEE Trans. Power Syst.*, vol. 32, no. 2, pp. 1578–1579, Mar. 2017.

[16] W. Li, Y. Wang, and T. Chen, "Investigation on the Thevenin equivalent parameters for online estimation of maximum power transfer limits," *IET Gener., Transmiss. Distrib.*, vol. 18, no. 1, pp. 121–127, Feb. 2010.

[17] W. Xu, I. R. Pordanjani, Y. Wang, and E. Vaahedi, "A network decoupling transform for phasor data based voltage stability analysis and monitoring," *IEEE Trans. Smart Grid*, vol. 3, no. 1, pp. 261–270, Mar. 2012.

[18] Y. Wang, I. R. Pordanjani, W. Li, W. Xu, T. Chen, E. Vaahedi, and J. Gurney, "Voltage stability monitoring based on the concept of coupled single-port circuit," *IEEE Trans. Power Syst.*, vol. 26, no. 4, pp. 2154–2163, Nov. 2011.

[19] H. Yaghobi, "A new adaptive impedance-based LOE protection of synchronous generator in the presence of STATCOM," *IEEE Trans. Power Del.*, vol. 32, no. 6, pp. 2489–2499, Dec. 2017.

[20] A. Nassaj and S. M. Shahrtash, "An accelerated preventive agent based scheme for postdisturbance voltage control and loss reduction," *IEEE Trans. Power Syst.*, vol. 33, no. 4, pp. 4508–4518, Jul. 2018.

[21] H. Xiao, Y. Li, D. Shi, J. Chen, and X. Duan, "Evaluation of strength measure for static voltage stability analysis of hybrid multi-infeed DC systems," *IEEE Trans. Power Del.*, vol. 34, no. 3, pp. 879–890, Jun. 2019.

[22] J.-H. Liu and C.-C. Chu, "Wide-area measurement-based voltage stability indicators by modified coupled single-port models," *IEEE Trans. Power Syst.*, vol. 29, no. 2, pp. 756–764, Mar. 2014.

[23] J. H. Liu and C.-C. Chu, "Long-term voltage instability detections of multiple fixed-speed induction generators in distribution networks using synchrophasors," *IEEE Trans. Smart Grid*, vol. 6, no. 4, pp. 2069–2079, Jul. 2015.

[24] H. Yuan, X. Li, F. Li, X. Fang, H. Cui, and Q. Hu, "Mitigate overestimation of voltage stability margin by coupled single-port circuit models," in *Proc. IEEE Power Energy Soc. Gen. Meeting (PESGM)*, Jul. 2016, pp. 1–5.
[25] T. Sun, J. Liu, C. Li, S. Song, and Y. Yang, "An analytic method to calculate Thévenin equivalent parameters using single-time wide area PMU measurements," in *Proc. 2nd IEEE Conf. Energy Internet Energy Syst. Integr.*, Oct. 2018, pp. 1–5.
[26] H.-Y. Su and C.-W. Liu, "Estimating the voltage stability margin using PMU measurements," *IEEE Trans. Power Syst.*, vol. 31, no. 4, pp. 3221–3229, Jul. 2016.
[27] H.-Y. Su, "An efficient approach for fast and accurate voltage stability margin computation in large power grids," *Appl. Sci.*, vol. 6, no. 11, pp. 1–17, Nov. 2016.
[28] T. S. K. Reddy and R. Sunitha, "Estimation of voltage stability margin using impedance matching method," in *Proc. Int. Conf. Energy, Commun., Data Anal. Soft Comput.*, Aug. 2017, pp. 1996–2002.
[29] A. Chandra and A. K. Pradhan, "Online voltage stability and load margin assessment using wide area measurements," *Int. J. Electr. Power Energy Syst.*, vol. 108, pp. 392–401, Jun. 2019.
[30] T. L. Baldwin, L. Mili, M. B. Boisen, Jr., and R. Adapa, "Power system observability with minimal phasor measurement placement," *IEEE Trans. Power Syst.*, vol. 8, no. 2, pp. 707–715, May 1993.
[31] P. Zhu, G. Taylor, and M. Irving, "Performance analysis of a novel *Q*-limit guided continuation power flow method," *IET Gener. Transmiss. Distrib.*, vol. 3, no. 12, pp. 1024–1051, 2009.

JIAN-HONG LIU (Member, IEEE) was born in Taipei, Taiwan, in 1983. He received the B.Sc. degree from Tatung University, Taipei, the M.Sc. degree from the National Cheng Kung University (NCKU), Tainan, Taiwan, and the Ph.D. degree from the National Tsing Hua University (NTHU), Hsinchu, Taiwan, in 2006, 2008, and 2014, respectively, all in electrical engineering.

He is currently an Assistant Professor of electrical engineering with Yuan Ze University (YZU), Taoyuan, Taiwan. His research interests include PMU applications to transmission capability assessment of renewable energy and voltage stability.

JIE-SHENG CHENG was born in Yunlin, Taiwan, in 1996. He received the B.Sc. degree in electrical engineering from Feng Chia University (FCU), Taichung, Taiwan, in 2018. He is currently pursuing the M.Sc. degree with Yuan Ze University (YZU), Taoyuan, Taiwan. His research interests include voltage control and monitoring of distributed generators.